Numerical study on a boundary layer control system and vortex generator to alleviate a static pressure gradient

Seung Hun Lee, Ju Yeol You and Yongmin Park

Aerodynamics Development Team
Hyundai Motor Group
150, Hyundaiyeonguso-ro, Namyang-eup
Hwaseong-si, Gyeonggi-do, 18280, Korea

seunghun.lee@hyundai.com
aerodoctor@hyundai.com
parkie94@hyundai.com

Abstract: A primary distributed suction located at the close upstream of center-belt in HAWT (Hyundai Aero-acoustic Wind Tunnel) has been a major source of static pressure gradient inside a plenum. This gradient, however, is further augmented by a vortex generating (VG) system, which has been installed recently to mitigate aerodynamic data fluctuations. To alleviate the steep static pressure gradient, an optimal configuration of a boundary layer control system is investigated numerically regarding the static pressure gradient as well as the corresponding boundary layer thickness inside the plenum. Various configurations are investigated for the primary suction and scoop, secondary tangential blowing slot. With the combination of the primary suction (or scoop) and tangential blowing slot, a flatter static pressure gradient is obtained without sacrificing a boundary layer thickness compared to the current configuration. Secondly, a new VG configuration with less deviation in static pressure gradient is suggested by numerical investigations. In terms of reducing the aerodynamic data fluctuation, this new VG is experimentally proven to show comparable performance to the original VG.

1 Introduction

To have better simulation in open-jet automotive wind tunnels, flow qualities such as pressure fluctuation, boundary layer thickness and static pressure gradient in the plenum have been of great interest for aerodynamic engineers [1-6]. The Hyundai Aero-acoustic Wind Tunnel (HAWT) has been placed in operation since 1999 [2] and has been suffering from the flow quality problems. In 2000, for instance, unexpected pressure fluctuations were found at initial commissioning tests and a structural modification in a collector was followed [3]. Even though the pressure fluctuations were fairly mitigated after this corrective work, they still exist today. The second problem is the negative static pressure gradient inside the test section. In HAWT, the boundary layer is solely controlled by the primary and secondary distributed suctions at the close upstream of the moving ground system. This suction-dependent system has been a major source of the steep negative static pressure gradient in the test section, which has restricted any upgrade accompanying a side effect on the static pressure gradient.

For instance, a vortex generating system (VG) on a nozzle lip is experimentally proven to mitigate the low frequency data fluctuations, which halves the required data recording time (figure 1) [1]. However, the negative axial static pressure gradient within the plenum is increased by the VG, and a vehicle surface pressure is changed correspondingly (figure 1*c*). With the change in the axial static pressure gradient, the drag coefficient of a vehicle increases, and some aerodynamic parts show different effects on the drag coefficient. This is one of the reasons for an automotive wind tunnel to make the static pressure gradient as flat as possible. Therefore, the use of the VG in HAWT has been considered unacceptable.

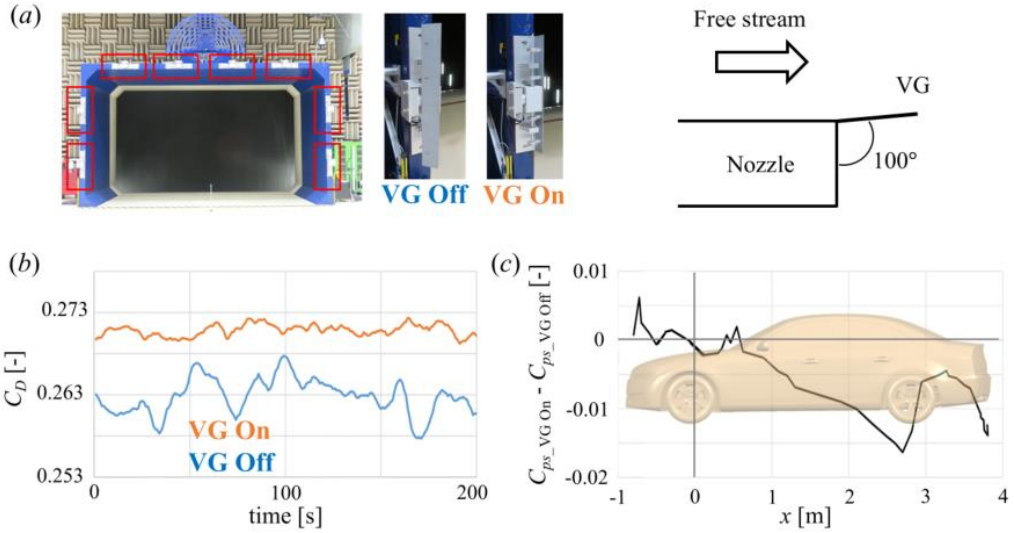

Figure 1. (a) Retractable vortex generators (VG) on the nozzle lip and its schematics. (*b*) Time histories of the drag coefficient and (*c*) deviation in the static pressure coefficient on the upper surface at y=0 of a DrivAer notchback model [1]

In this study, the vortex generating system (VG) is installed in a virtual HAWT model despite its negative impact on the steep static pressure gradient. After then, alternative boundary layer control layouts are numerically investigated to alleviate the steep static pressure gradient, without sacrificing the boundary layer thickness. The investigated alternative layouts are inspired by the novel designs of the state-of-the-art automotive wind tunnels [7-12]. Additionally, the static pressure gradients in the plenum are investigated for alternative VG configurations. A sophisticated virtual wind tunnel geometry and associated numerical schemes to assess wind tunnel interference effects such as the static pressure gradient and boundary layer thickness are introduced as well.

2 Numerical Setup

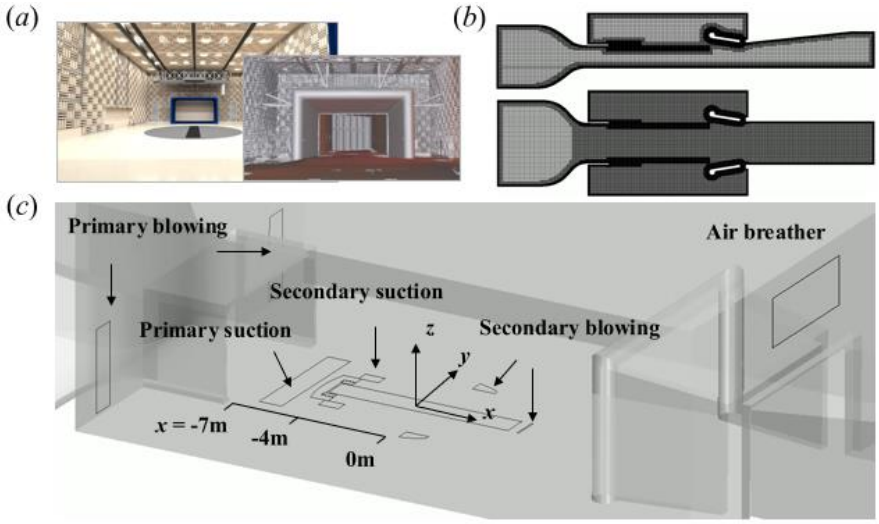

Figure 2. (*a*) Reconstruction of three-dimensional CAD geometries of HAWT. (*b,c*) Computational domain and grid systems. Note that secondary suction and blowing are not activated in this study

As a first step toward building the virtual wind tunnel, the three-dimensional CAD geometries of the entire circuit are reconstructed from the old blueprints written in the 90's. Missing parts and details are supplemented by the point cloud data measured from a state-of-the-art three-dimensional laser scanner (figure 2*a*).

For the investigation on the flow physics in the plenum, the computational domain can reasonably be reduced to the settling chamber with contraction, the first high-speed diffuser and the plenum with its appendages. In the plenum of computational domain, the center-belt of the moving ground system, the primary distributed suction, and the VG at the nozzle lip are considered (figures 2*b,c*). The air removed by the primary suction is reinjected to the plenum through blowing slots at the wall behind the nozzle. Even though HAWT has the secondary distributed suction and associated blowing slots, they are not activated in this study due to their minor impact on the negative axial static pressure gradient and the boundary layer thickness.

The governing equations for the 3-D incompressible turbulent flow in the virtual wind tunnel are solved numerically using a STAR-CCM+ with the built-in standard steady-state K-Omega SST turbulence model with all y^+ treatment. The so-called coupled implicit solver with the implicit spatial integration using a coupled algebraic multi-grid method is implemented, and the convective and diffusion terms are discretized by the second-order upwind scheme. At the boundaries, a boundary-normal mass flow condition is applied to the blowing slots, circuit inlet and outlet. A slip wall with prescribed boundary-normal velocity is imposed for the distributed suction, and a convective outflow boundary condition with gauge pressure of 0Pa is applied to the air breather above the collector flap. The no-slip condition is imposed on the rest of boundaries (figure 2*c*).

The trimmed cell type grids with 10 prism layers are imposed on all the surfaces except for the high-speed diffuser, the side walls and ceiling of the plenum. The first grid height is small enough to insure the y^+ value below unity at 140kph, and the longitudinal size of surface grid ranges from 3 to 30mm (figure 2*c*). The maximum volumetric grid size is 256mm. A grid convergence test is conducted to ensure less numerical errors, especially for the boundary layer and static pressure gradient.

For validation of the current numerical method, the calculated boundary layer profile and the axial static pressure gradient are compared with those of the experimental results (figure 3). Unless otherwise noted throughout the study, they are measured at the middle of center-belt (x=0m) and 0.6m above the ground (z=0.6m), respectively. Note that despite the secondary distributed suction with its associated blowing slots are excluded throughout this study, they are included in the present validation case because this is the test standard of HAWT. The calculated results are in excellent agreement with those of the experimental results, confirming the validity of the current model. The numerical model well captures the change in negative axial static pressure gradient by the VG (figures 3*b*,*c*).

Note that the δ_{99} value of the case without the secondary boundary layer treatment will be globally used in normalizing all the heights in the boundary layer profile throughout the paper. For instance, the boundary layer thickness of the standard experimental case with primary and secondary treatments is calculated to be $0.92\delta_{99}$. Likewise, the ΔC_{ps0} value along the center-belt (-4m to 4m) of the case with VG and without secondary boundary layer treatment is used to normalize the static pressure gradient.

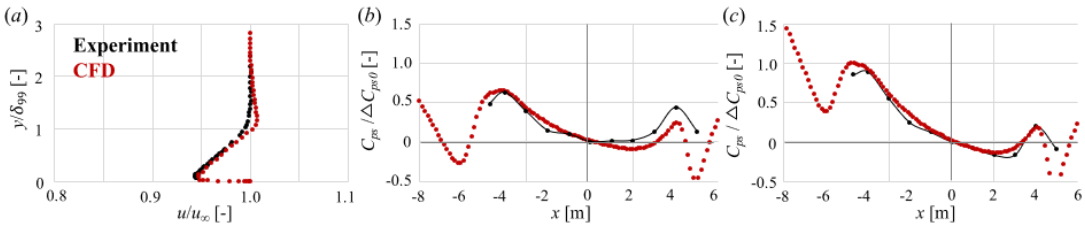

Figure 3. (*a*) Boundary layer profiles at x=0m without the VG. Axial static pressure gradients at z=0.6m without (*b*), and with (*c*) the VG

3 Investigation on Boundary Layer Control Systems

3.1 Primary suction

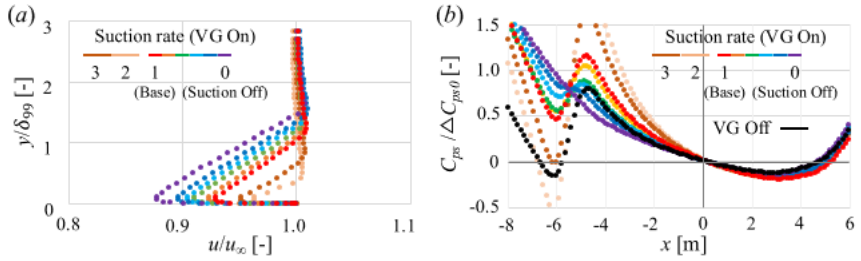

Figure 4. (*a*) Boundary layer profiles at x=0m and (*b*) axial static pressure gradients at z=0.6m for the different suction mass flow rates

As described in the introduction, the VG increases the negative static pressure gradient. With the existence of the current unmodified primary distributed suction, the VG increases ΔC_{ps} value along the center-belt (-4m to 4m) from -0.69 to -1.0ΔC_{ps0}. This chapter will show that the increased ΔC_{ps} value can be decreased by manipulating the total mass flow rate, location, and size of the primary suction [7-10].

The mass flow rate of the current unmodified position is investigated first, which can be the easiest test case in the real world. However, when the negative static pressure gradient becomes less steep, the boundary layer thickness becomes large, and vice versa (figure 4). For example, reducing the suction mass flow rate from 1 to 0.4~0.6 reduces the ΔC_{ps} value along the center-belt from -1.0 to -0.69ΔC_{ps0} (figure 4*a*). However, it increases the boundary layer thickness from 1.0 to 1.21δ_{99} (figure 4*b*). In a similar way, tripling the suction mass flow rate effectively reduces the boundary layer thickness from 1.0 to 0.35δ_{99}, while increasing the ΔC_{ps} value along the center-belt from -1.0 to -1.60ΔC_{ps0} (figures 4*a,b*). Therefore, adjusting the suction mass flow rate is not acceptable.

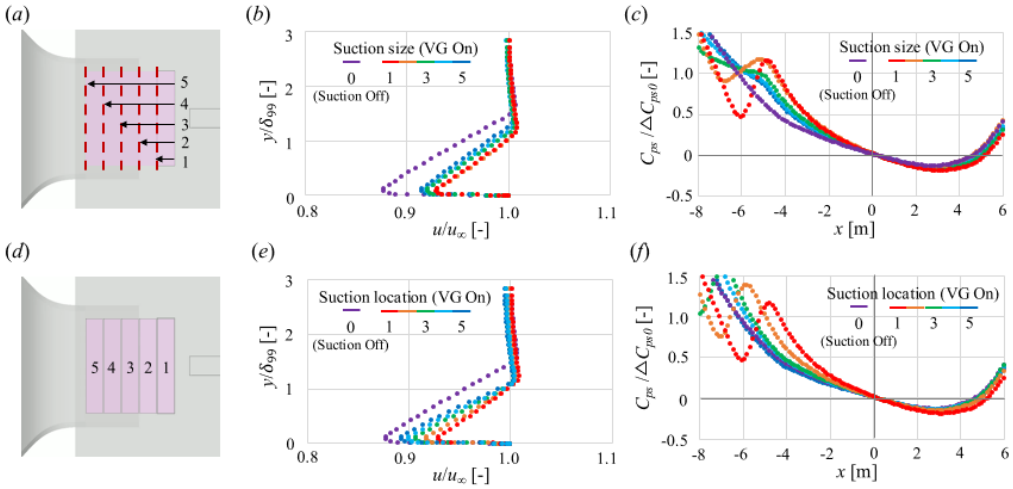

Figure 5. The (*a*) increase in size, and (*b*) change in location of the primary suction. (*b,e*) Boundary layer profiles at x=0m and (*c,f*) axial static pressure gradients at z=0.6m for (*a*) and (*b*), respectively

The recent automotive wind tunnels usually have large suction area to avoid strong suction velocity near the test section [7-10]. Here, the size of the primary distributed suction is extended toward the nozzle exit plane, and the total suction mass flow amount is not changed (figure 5*a*). The increase in primary distributed suction size does not decrease the boundary layer thickness (figure 5*b*) and has limited effect on the mitigation of the negative axial static pressure gradient (figure 5*c*). For example, with the increase in the size from 1 to 5, the ΔC_{ps} value along the center-belt (x=-4m to 4m) is reduced from -1.0 to -0.69ΔC_{ps0}. Note that the corresponding ΔC_{ps} value of the case with no suction is -0.50ΔC_{ps0}. Although the data are not presented here, increasing the suction mass flow rate for the extended suction size is not acceptable due to an excessive negative axial static pressure gradient.

The next step is to move the primary distributed suction toward the nozzle. In this case, the size of the suction plate and total suction mass amount are not changed. Interestingly, the boundary layer thickness remains nearly constant regardless of the suction plate position (figures 5*d*,*e*). Moving toward the upstream reduces the flow speed inside the boundary layer, which results in slight increase in the displacement thickness. Because the position 5 is far from the test section, the axial static pressure gradient is almost identical to that of the case with no suction (figure 5*f*).

Also, a reason for the upstream suction position can be found in the boundary layer profiles of the case without no suction. Here, the boundary layer thickness at the contraction exit (x=-10m) is already almost half of that at the leading edge of the center-belt (x=-4m) (figure 6). Therefore, the primary suction should be located inside the nozzle (i.e. position 5) exit plane to remove this already-grown local boundary layer. The regrowth of the boundary layer after the primary suction can be removed by secondary or tertiary boundary layer treatment [7-12].

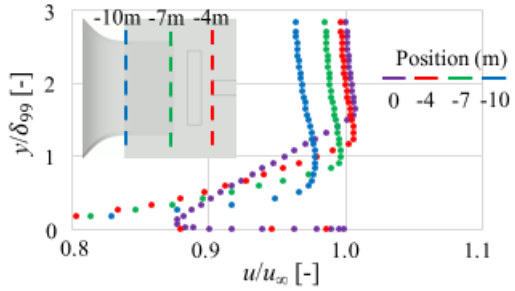

Figure 6. Boundary layer profiles of the case with no suction at x=-10, -7, -4 and 0m

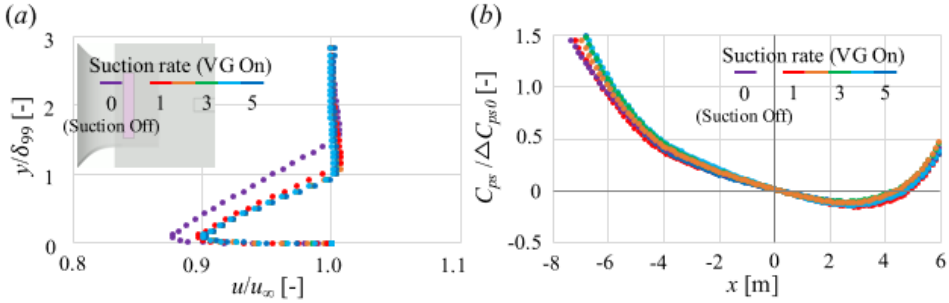

Figure 7. (*a*) Boundary layer profiles at x=0m and (*b*) axial static pressure gradients at z=0.6m for the primary suction in position 5 of figure 5*d*

Finally, the suction mass flow rate at the far upstream (i.e. position 5 of figure 5*d*) is investigated (figure 7). Note that the increase in the suction mass flow rate at the close upstream of the center-belt (position 1 of figure 5*d*) has proven to be unacceptable due to the excessive negative axial static pressure gradient (figure 4).

At position 1, the boundary layer thickness is effectively reduced by increasing the suction mass flow rate. For instance, tripling the suction mass flow rate reduces the boundary layer thickness from 1.0 to $0.35\delta_{99}$ (figure 4*a*). At position 5, however, the boundary layer thickness is not effectively reduced by the increase in the suction mass flow rate. For example, tripling the suction mass flow rate merely reduces the boundary layer thickness from 1.16 to $1.0\delta_{99}$ (figure 7*a*). These results indicate that the current suction mass flow rate is enough to remove all the local boundary layer at position 5. Without the boundary layer control, note that the boundary layer thickness at x=-10m is half of that at x=-4m (figure 6). Admittedly, the axial static pressure gradient at the test section is not affected by the increase in the suction mass flow rate (figure 7*b*).

3.2 Primary scoop

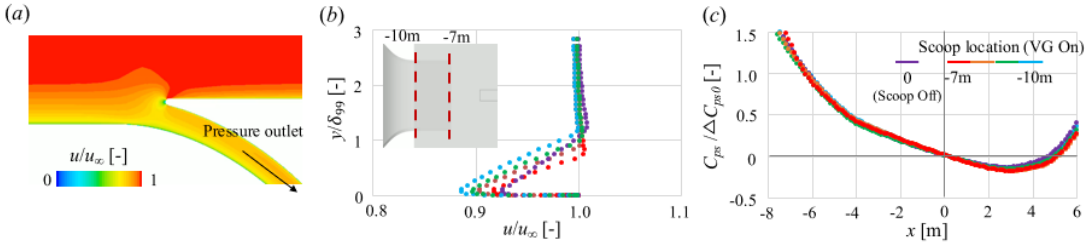

Figure 8. (*a*) Velocity contour around a primary scoop. (*b*) Boundary layer profiles at x=0m and (*c*) axial static pressure gradients at z=0.6m for the different scoop locations

In this chapter, a primary scoop with a passive convective outflow boundary condition with gauge pressure of 0Pa is employed (figure 8*a*). According to the previous studies [6,12], the scoop should be located inside the nozzle exit plane to avoid pressure interference from a vehicle. Because the boundary layer thickness at the nozzle exit plane (x=-7m) is approximately $0.92\delta_{99}$ (figure 6*a*), the scoop with width of $1.0\delta_{99}$ is representatively investigated for the various locations from x=-7m to -10m. It is obvious that the boundary layer removal becomes effective as the scoop moves close to the test section (figure 8*b*). The scoop itself, regardless of its location, does not affect the axial static pressure gradient within the test section (figure 8*c*). With the scoop at x=-7m, the boundary layer thickness is $0.75\delta_{99}$. This value is remarkably small since the boundary layer thickness with the primary suction at the similar location is greater than $1.0\delta_{99}$ (figure 5*e*).

Although the data are not presented here, the scoop with width of $0.5\delta_{99}$ is not enough to remove all the boundary layer at x=-7m. On the other hand, the scoop with width of $1.5\delta_{99}$ is redundant and has a similar boundary layer removal performance of the scoop with width of $1.0\delta_{99}$.

3.3 Tangential blowing

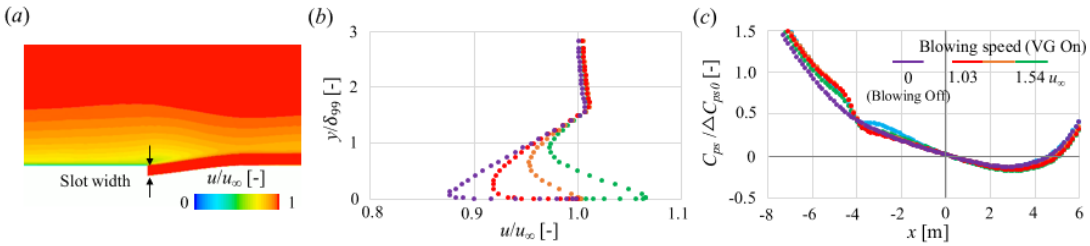

Figure 9. (*a*) Velocity contour around the tangential blowing slot. (*b*) Boundary layer profiles at x=0m and (*c*) axial static pressure gradients at z=0.6m for the slot width of $0.10\delta_{99}$

A lot of modern automotive wind tunnels employ a tangential blowing system as a supplementary boundary treatment [7-12]. As a preliminary study, a tangential blowing slot at the leading edge of the center-belt (x=-4m) is introduced without other boundary layer control systems. The slot span length in y-direction equals to the length of the nozzle. The x-directional length is one tenth of that in y-direction. The bottom surface within the slot asymptotically matches the test section ground (figure 9*a*). Considering the previous theoretical and experimental studies [4,5,13], the slot width of 0.05, 0.10, $0.20\delta_{99}$ and the blowing speed of 1.03, 1.29, $1.54u_\infty$ are considered.

The results for the slot width of $0.10\delta_{99}$ are representatively presented in figures 9*b*,*c*. With the tangential blowing, the boundary layer displacement thickness is decreased due to the increase in the velocity near the ground (figure 9*b*). However, the boundary layer thickness itself is rarely affected by the tangential blowing because the blowing jet is not fully mixed throughout the entire height of the boundary layer [4,13], which is why the tangential blowing should be used in conjunction with the primary boundary layer control system.

In this slot width, the proper blowing speed is around $1.29u_\infty$ to prevent velocity overshoot near the ground. As investigated previously [4,5], the associated static pressure gradient deviation is limited compared to that of the suction (figure 9*c*). For example, the ΔC_{ps} values along the center-belt (x=-4 to 4m) are $-0.46\Delta C_{ps0}$ and $-0.50\Delta C_{ps0}$ for with and without tangential blowing, respectively. Although the data are not presented here, the blowing speed needs to be higher for the smaller slot width. Further studies are needed to optimize the curvature within the slot, which is believed to affect the mixing behavior of the blowing jet within the boundary layer.

3.4 Combined boundary layer control system

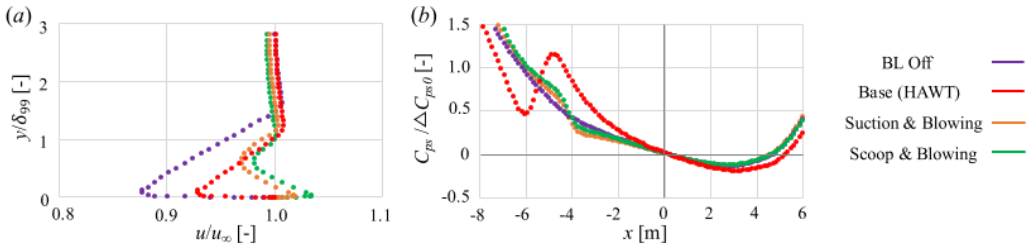

Figure 10. (*a*) Boundary layer profiles at x=0m and (*b*) axial static pressure gradients at z=0.6m

Finally, an optimal boundary layer control system in HAWT is realized by combining the primary suction or scoop with the secondary tangential blowing, which has already been demonstrated in the modern automotive wind tunnels [7-12]. From the conclusions above, the best options of each system are selected and representatively investigated. For instance, the upstream primary distributed suction (i.e. position 5 in figure 5*d*) with the current basic suction mass flow is considered. For the primary scoop, the width is $1.0\delta_{99}$ and the location is at the nozzle exit plane (x=-7m) (figure 8*b*). The width of tangential blowing slot is $0.10\delta_{99}$ and the blowing speed is $1.29u_\infty$.

The combined system of the primary suction or scoop with the tangential blowing shows the boundary layer thickness around $0.92\sim1.0\,\delta_{99}$ (figure 10*a*), which is comparable to the value of the current basic configuration ($1.0\delta_{99}$). Moreover, with the mass and momentum supplied from the tangential blowing, the boundary layer displacement thickness is significantly reduced. The displacement thicknesses are $0.042\,\delta_{99}$ and $0.016\,\delta_{99}$, respectively, for the current basic configuration and the primary suction with tangential blowing configuration. Even though the boundary layer (displacement) thickness is not sacrificed, the axial static pressure gradient becomes significantly flat. The ΔC_{ps} values along the center-belt (x=-4m to 4m) are $-0.46\Delta C_{ps0}$ and $-0.42\Delta C_{ps0}$ respectively for those with the primary scoop and suction, which are even lower than that from the case without the boundary layer control system ($\Delta C_{ps} = -0.50\Delta C_{ps0}$).

4 Investigation on a new VG Design

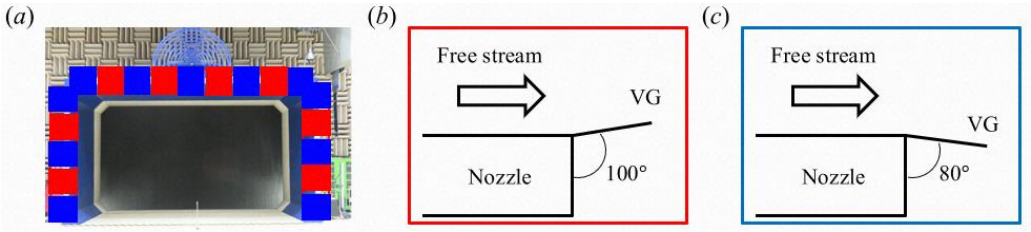

Figure 11. (*a*) The nozzle of HAWT. In red and blue regions, (*b*) inward and (*c*) outward vortex generating plates are respectively positioned

In addition to the investigation on the boundary layer control system, this chapter focuses on finding an alternative VG configuration whose associate negative static pressure deviation is less than the current VG. The current VG consists of flat plates, which are tilted 10˚ toward the free steam (figures 1*a*, 11*b*). This configuration squeezes the free stream and causes the augmentation of negative static pressure gradient in the test section. To the best of authors knowledge, the reason for the deviation in static pressure gradient under this configuration is not clear. After all, a new VG design is employed not to squeeze the free stream. Therefore, outward-tilting plates are additionally considered (figure 11*c*). Refer to the positions of inward- and outward-tilting plates at the nozzle lip in figure 11.

In this study, inward-only and outward-only VGs are respectively considered. The ($\Delta C_{ps}/\Delta C_{ps0}$, $\Delta u/u_\infty$) values along the center-belt (x=-4m to 4m) of inward and outward VGs are (-1.0, 0.013) and (-0.57, 0.003) respectively (figures 12*a*,*b*). Note that the corresponding (ΔC_{ps}, $\Delta u/u_\infty$) values of no-VG case are (-0.69, 0.007). These results indicate that the outward VG case shows a flatter static pressure and velocity gradient in the test section than those of inward VG and no-VG cases.

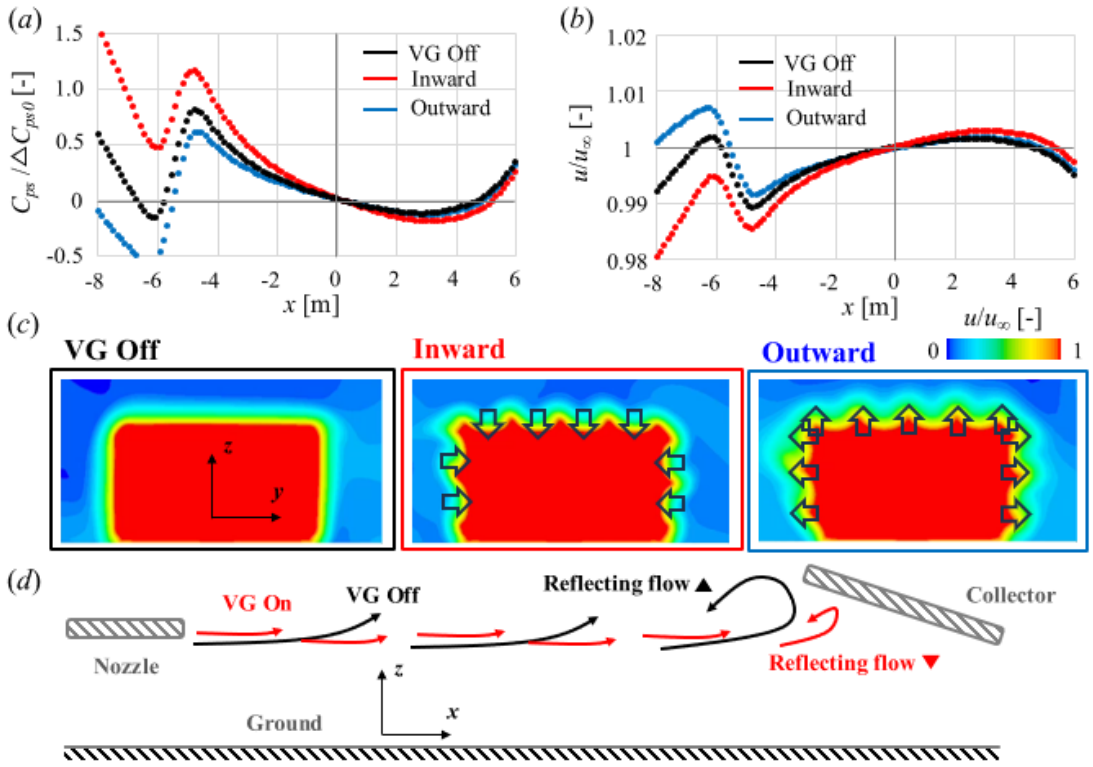

Figure 12. (*a*) Axial static pressure gradients and (*b*) velocity profiles at z=0.6m. (*c*) Velocity magnitude contours at x=0. The location and direction of arrows in (*c*) indicate the position and tilted direction of the vortex generating plates, respectively. (*d*) Schematic diagram of shear layer behaviors in open-jet test section

In no-VG case, large-scale coherent shear layer vortices are developed along the smooth perimeter of nozzle outlet. For instance, coherent z- and y-directional vortices are respectively observed for the lateral and upper sides of free stream jet boundary in no-VG case (figures 12*c*,*d*). These large-scale vortices are reflected by collector flaps and cause data fluctuation [1,2]. The primary purpose of VG is to dissipate these large-scale vortices into smaller pieces, thereby reducing the reflecting flow [1]. Interestingly, the coherent shear layer vortices disappear for both cases with inward and outward VGs (figure 12*c*). Small staggered vortical structures are presented along the free stream jet boundary, instead. Since the inward VG has experimentally been proven to mitigate data fluctuations, the outward VG is expected to show a similar effect.

However, the numerical investigation on unsteady data fluctuations with VG is limited since the current numerical scheme employes the steady-state solver. An unsteady numerical scheme needs to be developed and validated in the near future. In this study, experimental investigations on the unsteady characteristics of VG are presented alternatively.

Figure 13. VG and pitot tude set-up in HAWT

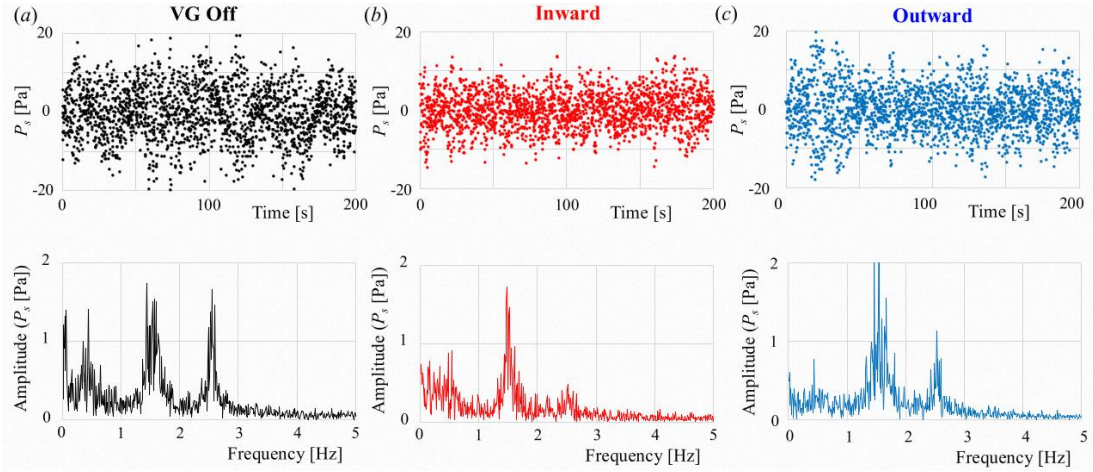

Figure 14. Time histories of static pressure at 0.6m above the middle of center-belt and their FFT results with (*a*) no-VG, (*b*) inward VG, (*c*) and outward VG

For the experiments, inward and outward VGs were installed on the nozzle lip of HAWT. With a pitot tube, time histories of static pressure at 0.6m above the middle of center-belt were measured for no-VG, inward VG, and outward VG cases (figures 13,14). In case of no-VG, the dominant frequencies of the static pressure fluctuation occur at around 0.5, 1.5 and 2.5Hz. On the other hand, the inward VG reduces the magnitude of dominant frequencies at 0.5 and 2.5Hz. The outward VG also reduces the dominant peaks at both 0.5 and 2.5Hz, but the magnitude at 2.5Hz is greater than the case with inward VG.

Especially, the reduction in the peak at 0.5Hz is an encouraging result since the required data acquisition time depends on the fluctuation in lowest frequency. As the inward VG halves the required data acquisition time, a similar effect is expected with the outward VG. To validate this assumption, drag fluctuations of DrivAer model with outward VG will soon be conducted.

5 Concluding remarks

A vortex generator (VG) on the nozzle lip was developed to reduce the fluctuation in aerodynamic data but the application of it has been limited because it increases the negative static pressure gradient. To alleviate the increased negative static pressure gradient by VG, alternative boundary layer control systems are numerically investigated. A far upstream primary distributed suction (or scoop) with secondary tangential blowing near the test section shows the most flatest static pressure gradient, without sacrificing the boundary layer thickness. Secondly, the new VG configuration is suggested by numerical simulation and is validated by experiment. This VG reduces the fluctuation in the aerodynamic data and shows the minimal deviation in the negative static pressure gradient. The combination of the new boundary layer control systems and new VG will help HAWT to have better flow quality.

Throughout the study, the current numerical scheme is validated to capture the various wind tunnel interference effects. The application of this invaluable method will not be limited to the current study and will be expanded to understand other flow physics. For instance, correlation study on the wind tunnel and open road conditions will be an interesting research topic. In addition to the current steady-state scheme for the wind tunnel, an unsteady scheme is under development.

6 Reference list

[1] You, J. Y., Kwon, H. & Jeon, S. et al., 2023 Reduction of flow fluctuation with vortex generating system. Proceedings of FKFS Conference on Vehicle Aerodynamics and Thermal Management. 2023

[2] Kim, M., Lee, J., Kee, J. & Chang, J. 2001 Hyundai full scale aero-acoustic wind tunnel. *SAE Tech. Pap.* 2001-01-0629

[3] Rennie, M., Kim, M., Lee, J. & Kee, J. 2004 Suppression of open-jet fluctuations in the Hyundai aeroacoustic wind tunnel. *SAE Tech. Pap.* 2004-01-0803

[4] Berndtsson, A., Eckert, W. T. & Mercker, E. 1988 The effect of groundplane boundary layer control on automotive testing in a wind tunnel. *SAE Int. J. Passeng. Cars* 94, 215-230

[5] Mercker, E. & Wiedemann, J. 1990 Comparison of different ground simulation techniques for use in automotive wind tunnels. *SAE Tech. Pap.* 900321

[6] Wickern, G., Dietz, S. & Luehrmann, L. 2003 Gradient effects on drag due to boundary-layer-suction in automotive wind tunnels. *SAE Tech. Pap.* 2003-01-0655

[7] Buckisch, R., Schwartekopp, B. & Pfisterer, J. 2018 Diamler aeroacoustic wind tunnel: 5 years of operational experience and recent improvements. *SAE Tech. Pap.* 2018-01-5038

[8] Xu, L., Zhu, X., Wang, Q. & Bu, H. et al., 2025 The new China automotive engineering research institute co., Ltd full-scale aero-acoustic wind tunnel. *SAE Tech. Pap.* 2025-01-8779

[9] Waudby-Smith, P., Bender, T. & Sooriyakumaran, C. et al., 2024 The new China automotive technology and research center aerodynamic-acoustic and climatic wind tunnels. *SAE Tech. Pap.* 2024-01-2541

[10] Blumrich, R., Widdecke, N. & Wiedemann, J. et al., 2015 The new FKFS technology at the full-scale aeroacoustic wind tunnel of university of Stuttgart. *SAE Int. J. Passeng. Cars* 2015-01-1557

[11] Nagle, P., Brooker, T. & Bari, G. et al., 2023 The Ford rolling road wind tunnel facility. *SAE Tech. Pap.* 2023-01-0654

[12] Best, S., Bari, G. & Brooker, T. et al., 2023 The Honda automotive laboratories of Ohio wind tunnel. *SAE Tech. Pap.* 2023-01-0656

[13] Launder, B. E. & Rodi, W. 1979 The turbulent wall jet. *Prog. Aerosp. Sci.* 19, 81-128